Neutrino Oscillation Effects in Soudan-2 Upward-stopping Muons

W.W.M. Allison[3], G.J. Alner[4], D.S. Ayres[1], G.D. Barr[3], W.L. Barrett[6],
P.M. Border[2], J.H. Cobb[3], D.J.A. Cockerill[4], H. Courant[2], D.M. Demuth[2],
T.H. Fields[1], H.R. Gallagher[5], M.C. Goodman[1], T. Kafka[5],
S.M.S. Kasahara[2], P.J. Litchfield[2], W.A. Mann[5], M.L. Marshak[2],
W.H. Miller[2], L. Mualem[2], J.K. Nelson[2,a], A. Napier[5], W.P. Oliver[5],
G.F. Pearce[4], E.A. Peterson[2], D.A. Petyt[2], K. Ruddick[2], M. Sanchez[5,b],
J. Schneps[5], A. Sousa[5], J.L. Thron[1,c], N. West[3]

[1] *Argonne National Laboratory, Argonne, IL 60439*
[2] *University of Minnesota, Minneapolis, MN 55455*
[3] *Department of Physics, University of Oxford, Oxford OX1 3RH, UK*
[4] *Rutherford Appleton Laboratory, Chilton, Didcot, Oxfordshire OX11 0QX, UK*
[5] *Tufts University, Medford, MA 02155*
[6] *Western Washington University, Bellingham, WA 98225*

[a] Now at the College of William and Mary, Williamsburg, VA 23187.
[b] Now at Harvard University, Cambridge, MA 02138.
[c] Now at Los Alamos National Laboratory, Los Alamos, NM 87545.

February 7, 2008

Abstract

Upward-going stopping muons initiated by atmospheric ν_μ and $\overline{\nu}_\mu$ interactions in the rock below the Soudan 2 detector have been isolated, together with a companion sample of neutrino-induced single muons, created within the detector, which travel downwards and exit. The downward-going sample is consistent with the atmospheric-neutrino flux prediction, but the upward-going sample exhibits a sizeable depletion. Both are consistent with previously reported Soudan-2 neutrino-oscillation results. Inclusion of the two samples in an all-event likelihood analysis, using recent 3D-atmospheric-neutrino-flux calculations, reduces both the allowed oscillation parameter region and the probability of the no-oscillation hypothesis.

1 Introduction

The recently published neutrino oscillation analysis of the Soudan-2 atmospheric-neutrino data [1] used only Fully Contained (FC) events and Partially Contained (PC) events in which the neutrino interaction vertex was contained within the Soudan 2 tracking calorimeter. Not utilized by that study were two additional, topologically very similar, categories for which further analysis was needed to separate the samples and to eliminate their non-neutrino background. Using nomenclature introduced by the MACRO experiment [2], the two categories are labelled as *UpStop* events and *InDown* events.

UpStop events are upward-going stopping muons which arise from charged-current ν_μ and $\overline{\nu}_\mu$ interactions occurring in the rock surrounding the Soudan 2 cavern; only the final state muon is detected as a stopping, non-interacting track in the detector. The muon may be accompanied by a small number of hits from a decay electron near its stopping point.

InDown events are ν_μ and $\overline{\nu}_\mu$ interactions in the detector yielding downward going, exiting muons with three or fewer hits arising from hadronic track(s) at the production vertex. Approximately 65% of these InDown events are quasi-elastic interactions with low energy protons. Interactions having more than three hadronic hits at their primary vertex were included in the PC sample analyzed previously [1].

Separation of these two neutrino event samples is made possible by the fine-grain imaging of the Soudan-2 honeycomb-lattice tracking calorimeter. Their angular distributions exhibit features which are indicative of atmospheric $\nu_\mu \rightarrow \nu_\tau$ oscillations. The samples can be incorporated in a straightforward way into the likelihood analysis described in Ref. [1]. Their inclusion has enabled an improved determination of the $\nu_\mu \rightarrow \nu_\tau$ oscillation parameters from this experiment and a more stringent rejection of the no oscillation hypothesis.

Analyses of upward through-going muons [2, 3, 4, 5], and stopping muons [2, 4, 6, 7] have been previously reported. Whereas through-going muon samples originate from a broad high-energy neutrino spectrum having a mean E_ν of approximately 100 GeV, UpStop events originate predominantly from interactions with $1 \leq E_\nu \leq 20$ GeV. Consequently they provide different constraints for oscillation scenarios. Among the underground tracking calorimeter experiments, MACRO has provided the most detailed treatment to date of UpStop and InDown events. In that experiment it was not possible to separate the two categories, so they were analyzed as a combined sample. Clearly, it is advantageous to separate the samples, since comparison of their zenith angle distributions can provide additional discrimination between low ($\approx 10^{-3}$ eV^2) versus high ($\geq 10^{-2}$ eV^2) values of Δm^2.

2 Detector and data exposure

Soudan 2 was a 963 metric ton (770 tons fiducial) iron tracking calorimeter with a honeycomb geometry which operated as a time-projection chamber. The detector was located at a depth of 2070 meters–water–equivalent on the 27th level of the Soudan Underground Mine State Park in northern Minnesota. The calorimeter started data taking in April 1989 and ceased operation in June 2001 by which time a total exposure (fiducial exposure) of 7.36 kton-years (5.90 kton-years) had been obtained.

The calorimeter's tracking elements were 1 m long, 1.5 cm diameter hytrel plastic drift tubes filled with an argon-CO_2 gas mixture. The tubes were encased in a honeycomb matrix of 1.6 mm thick corrugated steel plates. Electrons deposited in the gas by the passage of charged particles drifted to the tube ends under the influence of an electric field. At the tube ends the electrons were amplified by vertical anode wires which read out a column of tubes. A horizontal cathode strip read out the induced charge and the third coordinate was provided by the drift time. The ionization deposited was measured by the anode pulse height. The calorimeter produced three-dimensional track hits with a spatial resolution of approximately 1 cm^3 and separated by an average of about 3 mm of steel. The corrugated plates, interleaved with drift tubes, were stacked to form 1×1×2.5 m^3, 4.3-ton modules from which the calorimeter was assembled in building-block fashion [8].

Surrounding the tracking calorimeter on all sides, but mounted on the cavern surfaces and well separated from the outer surfaces of the calorimeter, was a 1700 m^2 Veto Shield array of two or three layers of proportional tubes [9]. The shield recorded the presence of cosmic ray muons coincident in time with events in the main calorimeter and thus identified background events, either produced directly by the muons or initiated by secondary particles coming from muon interactions in the rock walls of the cavern. Additionally, for neutrino-induced muons which enter or exit the tracking calorimeter, the shield array recorded the muon in time-coincidence with the event in the central detector.

3   Separation of UpStop and InDown Events

The event imaging afforded by the Soudan 2 tracking calorimeter made it possible to distinguish the topologically similar UpStop and InDown events. Events of both types were isolated during routine processing.

Events were classified as UpStop candidates if they satisfied the following criteria:

(1) The track was muon-like, devoid of kinks or scatter vertices.

(2) The track length was greater than 100 cm.

(3) The muon endpoint occured in a live detector region. An event was removed if the candidate endpoint occured in the inactive region between modules.

(4) Track ionization and straggling were consistent with the hypothesis of an upward-going muon which ranges to stopping. That is, near the edge of the detector the track was straight and lightly ionizing while, near the interior end, the track exhibited multiple scattering and/or heavy ionization.

(5) Associated hits at the track endpoint, if any, had to be consistent with an electron shower from muon decay.

An anode-versus-cathode view of an UpStop data event is shown in Fig. 1 where multiple scattering can be discerned as the muon ranges to stopping. Endpoint decay hits, the three hits modestly displaced from the muon endpoint in Fig. 1, are observed in some events (with higher probability for μ^+ than for μ^- since the former do not undergo nuclear absorption within iron nuclei).
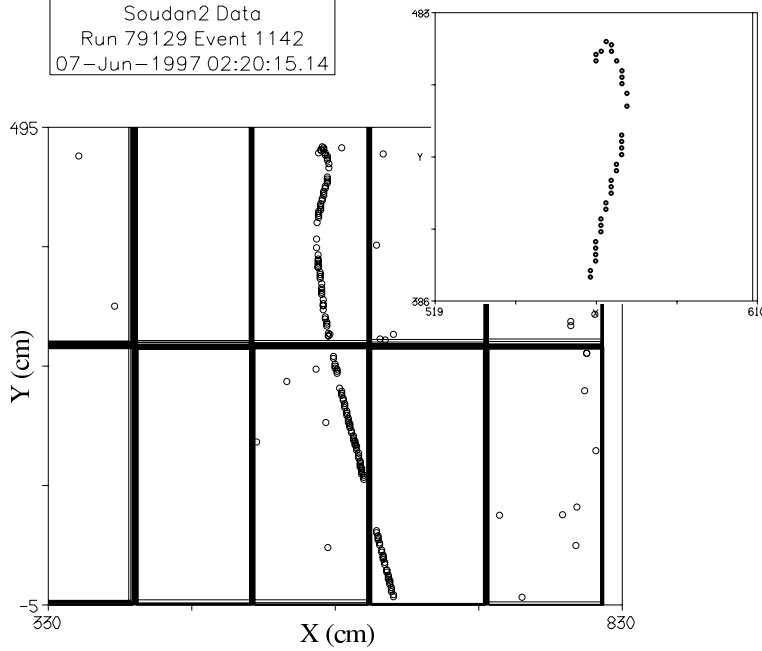
Figure 1: An UpStop data event recorded in the anode-cathode matched view (front view of the calorimeter). Typically, multiple scattering becomes pronounced as the muon approaches its range endpoint. The endpoint decay shower of three hits favors identification as a μ^+ rather than a μ^-.

InDown events were required to satisfy criteria 1-3 above and in addition:

(4) The muon track was straight and lightly ionizing at its interior end. Near the edge of the detector the track might, but need not, have exhibited ranging behavior in the form of multiple scattering and/or heavy ionization.

(5) Associated hits near the interior end of the track, if present, must have been consistent with hits from a proton or $\pi^\pm$ track, lying in a straight line and heavily ionizing.

These topological features are exhibited by the InDown data event shown in Fig. 2. At the event vertex, the muon is accompanied by a track of two hits for which the ionization is relatively heavy. This pattern is typical of a recoil proton. The event of Fig. 2 is a candidate quasi-elastic $\nu_\mu\, n \to \mu^- p$.

There were a few events which could not be resolved as UpStop or InDown, the direction of the track being undetermined. Fortunately, ambiguous cases were rare for tracks which have visible lengths exceeding one meter in the detector. For the purpose of analysis, such events were retained as an *Ambiguous* category.

4   Event processing and simulation

Both UpStop and InDown data events were selected in the Partially Contained event sample, and were processed as described in Ref. [1]. The Monte Carlo sample of the contained-vertex InDown events was also part of the routine data processing, in which Monte-Carlo events
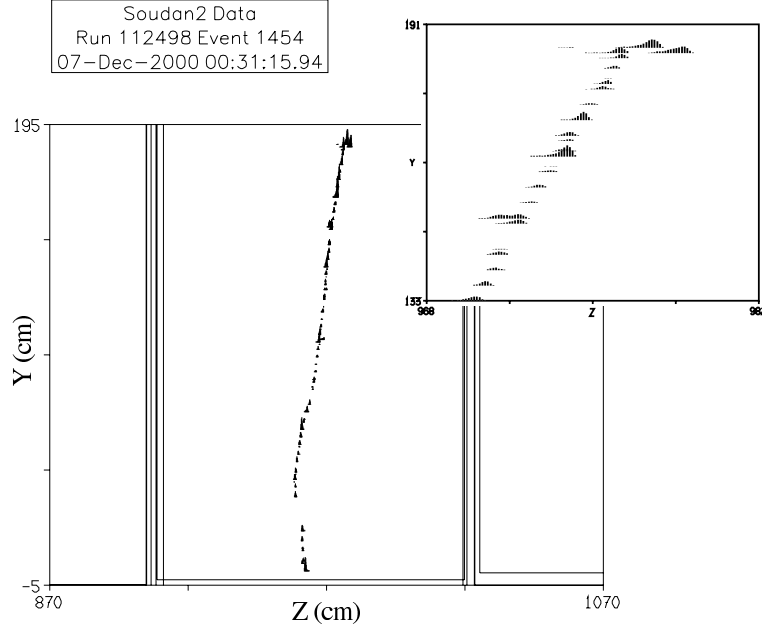
Figure 2: An InDown data event recorded in the cathode versus time view (calorimeter side view). The muon emerges from an event vertex which is well contained; its trajectory, a straight line initially, undergoes small angle deflection as the ranging muon approaches the detector floor. A proton recoil of two hits is visible at the vertex.

were inserted into and processed together with the data stream, their identity only being revealed in the final analysis stage. However, additional simulations, not included in the main data processing, were needed for the neutrino interactions in the rock surrounding the cavern, which give rise to UpStop events [10].

4.1 Simulation of upward-stopping muon events

The GEANT Monte Carlo program together with modified Soudan-2 software provided the UpStop simulation (UpStop-MC). A total of 68.7 million neutrino interactions in greenstone rock were simulated. The event vertices were distributed randomly through rock volumes which were centered on the Soudan 2 cavern. Since high-energy charged-current (CC) events can project muons to the cavern from more remote rock than low-energy events, the dimensions of the primary rock volumes were chosen to increase with increasing E_ν. Final-state particles were tracked through the rock by GEANT and fourvectors of particles that reached the veto-shield array were saved. These were then passed through the Soudan-2 Monte Carlo to produce realistic detector hits superimposed on detector noise represented by random-trigger records.

UpStop-MC events were then processed through the standard Soudan-2 triggering, reconstruction and selection software for PC events. For UpStop-MC events yielding ionization within the tracking calorimeter (71,000 events), the survival rates decreased monotonically with increasing primary E_ν, reflecting the diminishing probability for muons from energetic events to stop in the detector. Survival rates ranged from 12.8% for events with $E_\nu \leq 10$

GeV, to 2.5% for events with $E_\nu \geq 40$ GeV.

4.2 UpStop cuts and scanning

The PC selection filter required candidate tracks to penetrate to the fiducial region while not being through-going. Additional requirements, detailed in Ref. [1], were imposed in order to reject the high-flux background of downward-going cosmic-ray muons. A total of 7662 UpStop-MC events passed the filter and simulated trigger requirements. However, only 34% of these events yielded a potentially interesting topology in the detector. Consequently, additional cuts were applied to the true kinematic variables to reject those events which were certain not to pass the subsequent analysis cuts. These cuts (existence of a final-state muon with cosine zenith angle, $\cos \theta_z < +0.05$, and energy E_μ upon arrival at the detector within the range 350 MeV $< E_\mu < 3500$ MeV) were designed to ensure that the event had an upward-going muon that stopped within the calorimeter fiducial volume [10]. A 54% sample of the surviving events was then scanned by physicists, using scanning rules identical to those used for PC data event scanning. The additional criteria given in Sec. 3 were also applied to both data and MC events. All events which satisfied the scanning criteria were then reconstructed manually using the experiment's standard interactive graphics software. Only the reconstructed sample was used in the subsequent analysis. It contained a factor of 25 more events than the data sample.

4.3 MC event rate normalization

The atmospheric neutrino flux used to generate the UpStop events was the one-dimensional calculation of the Bartol group [11], modulated by the solar cycle as described in Ref. [1]. Other fluxes were simulated by applying correctional weights to the generated events. For consistency with Ref. [1], the numbers and plots in Sects. 5 and 6 were weighted to correspond to the updated 1D Bartol-96 flux [12]. The oscillation analysis of Sect. 7 of this paper used the latest three-dimensional fluxes from the Bartol group [13] and Battistoni *et al.* [14]. The neutrino cross sections were those encoded in NEUGEN3 [15]. The target nuclear composition was that of Soudan rock, described in Ref. [16]. The effect of Pauli blocking in elastic and quasi-elastic reactions was accounted for, however nuclear effects on resonance production and on deep inelastic scattering final states were neglected.

The event rate calculations have a sizable systematic error. For the comparison of this data with the MC presented in Sections 5 and 6, a normalization factor of 0.85, determined from the measured ν_e rate, assuming no oscillations, was applied. In the oscillation analysis described in Sec. 7 the overall normalization was a free "nuisance" parameter.

5 Event rates and backgrounds

5.1 Backgrounds in UpStop events

Two sources of background events were considered:

(1) Cosmic-ray muons which scatter in the rock and eventually enter the detector in an upward direction.

(2) Charged hadronic tracks, especially pions, produced at large angles in interactions of cosmic-ray muons in the rock surrounding the detector.

Unlike experiments which are situated under mountains, the flat overburden at Soudan ensures that the flux of cosmic-ray muons becomes less than the flux of neutrino-produced muons significantly above horizontal angles [16]. Thus the background from the first source is negligible.

Hadronic interactions of neutrons produced in cosmic ray interactions were shown in Ref. [1] to be a background to contained neutrino events. A similar, related, flux of charged hadrons also emerges from the cavern walls and enters the detector.

There are two distinguishing features of entering hadronic tracks:

(1) *Veto-Shield signal:* In addition to the Veto Shield hit corresponding to the passage of the hadron track, there are likely to be extra hits due to other particles produced in the muon interaction. In general, the track in the detector will not be aligned with these extra hits. It is thus useful to distinguish between the total number of in-time Veto Shield hits (n_{all}^{VS}) and the number of in-time hits geometrically associated with the incoming/leaving track (n_{trk}^{VS}).

(2) *Range:* Hadronic tracks have a limited range in the detector before stopping or interacting.
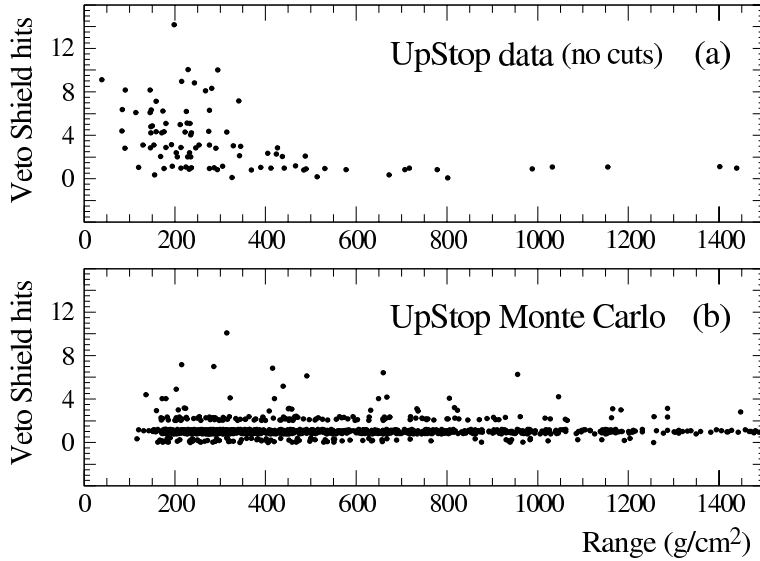

Figure 3: Distributions of Veto-Shield hit counts versus track range, (a) for UpStop data candidates and (b) for UpStop Monte Carlo events, prior to muon length cuts.

Fig. 3 shows n_{all}^{VS} versus the range of the stopping track for each event of the UpStop data (Fig. 3a) and of the MC (Fig. 3b). A clear excess of data events with large n_{all}^{VS} and small
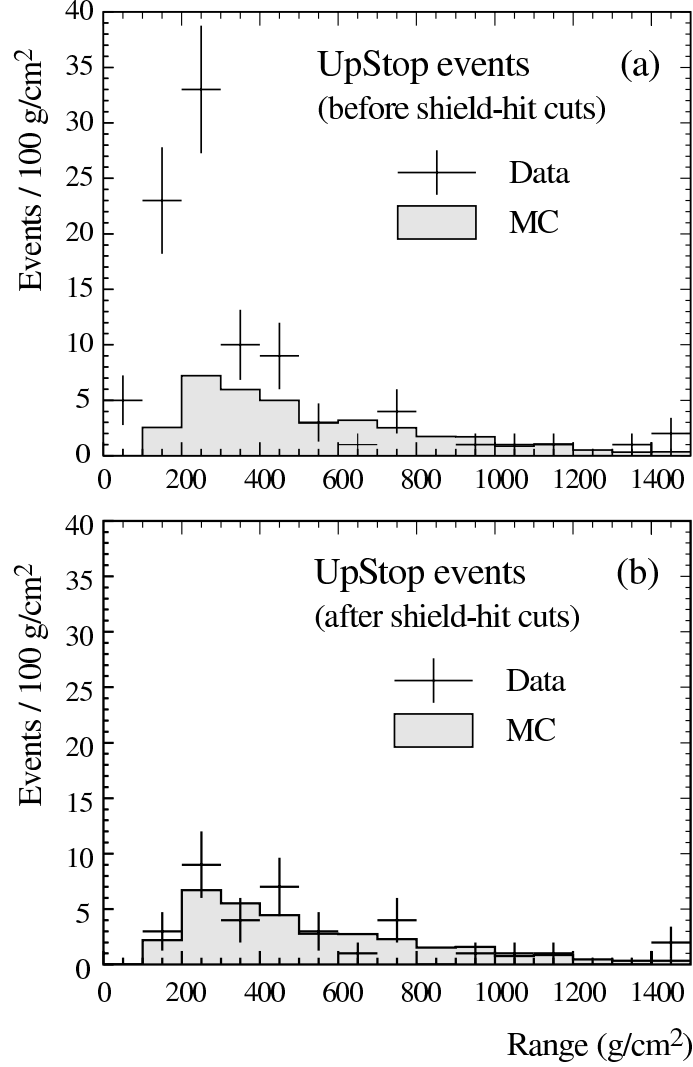
Figure 4: Distribution of track range for candidate UpStop data events (crosses) compared to the neutrino Monte Carlo sample (shaded histogram), for events with visible track length exceeding one meter. The distributions (normalized to the events with > 500 g/cm^2) are shown (a) before and (b) after the requirement $n_{all}^{VS} = n_{trk}^{VS}$ has been applied. Fig. 4b shows good agreement between the data and the neutrino MC.

range is observed, corresponding to the expectation for incoming hadronic tracks. However, at track lengths beyond the hadronic range, the data is consistent with the UpStop MC. The background signature is emphasized in Fig. 4a which shows the projection onto the range axis of the UpStop data (points with errors) and the MC (shaded histogram). The MC is normalized to the data with range > 500 g/cm^2 (> 3.8 pion interaction lengths). Fig. 4b shows the same distributions but with the additional constraint that $n_{all}^{VS} = n_{trk}^{VS}$, i.e. all Veto-Shield hits must be geometrically associated with the incoming track. The MC is then in good agreement with the data. However, to ensure that the residual hadronic background is negligible, a cut requiring the track range to be greater than 260 g/cm^2, corresponding to

two pion interaction lengths, is also applied. Since the calorimeter is, to good approximation, a uniform medium of 1.6 g/cm^3 density, the range requirement corresponds to a minimum track length requirement of $\sim$160 cm. The effective muon momentum threshold for UpStop and InDown events is $p_\mu \geq 530$ MeV/c.

Finally, the cosine of the zenith angle, $\cos\theta_z$, of the reconstructed UpStop track is required to be smaller than +0.05.

5.2 UpStop backgrounds using hadronic scatter events

The PC data analysis also recorded events with an incoming track making a hadronic scatter. A sample of 25 data events was obtained which can be used to gauge the background from incoming non-scattering hadrons. A representative event is the upward-going, stopping, charged pion track shown in Fig. 5. There are two coincident hits in the shield which are in close proximity to the track's entrance point into the cavern, hence $n_{trk}^{VS} = 2$. There is an additional coincident hit in the shield floor, hence $n_{all}^{VS} = 3$. Inside the detector, the track scatters and stops. The scatter, which gives rise to a recoil proton, plus the track ionization, identifies the track as a $\pi^\pm$ rather than a $\mu^\pm$ or a proton.
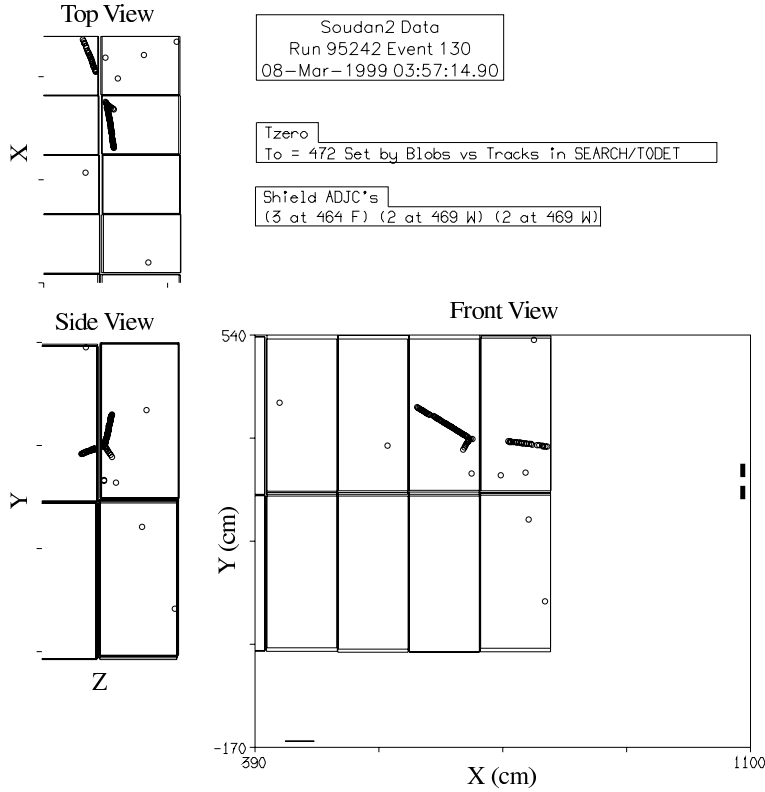

Figure 5: A scattering upgoing pion track (data event) accompanied by three time-coincident Veto Shield hits.

Distributions of $\cos\theta_z$ and of track range versus n_{all}^{VS} for the incoming hadronic sample are shown in Fig. 6. Fig. 6a shows that most of the events are downgoing. Among the seven
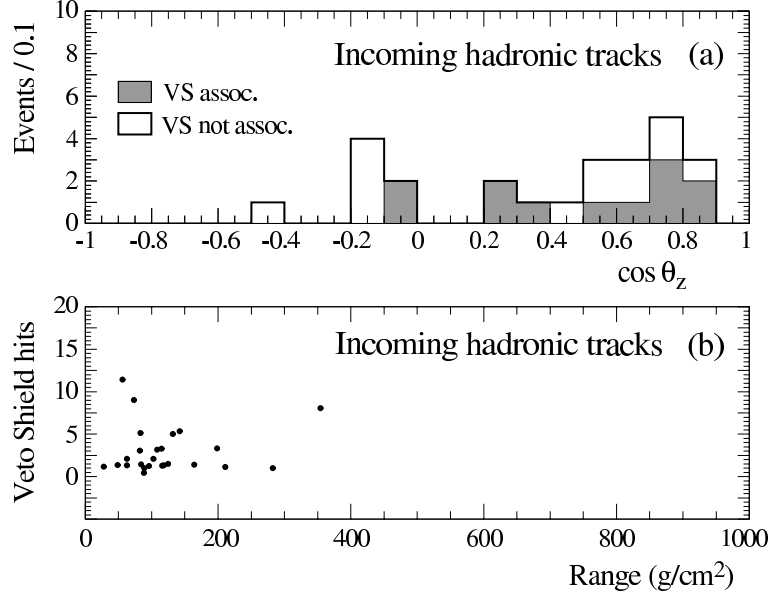
Figure 6: Distributions of (a) $\cos\theta_z$ and (b) the number of coincident veto shield hits versus the track range, for events which exhibit hadronic scatters. In Fig. 6(a), the shaded (open) histogram includes events where all the in-time Veto-Shield hits are (are not) associated with the detected track.

upward-going tracks, five have $n_{all}^{VS} > n_{trk}^{VS}$ (open histogram); the remaining two events with $n_{all}^{VS} = n_{trk}^{VS}$ (shaded histogram) are close to horizontal, and have short range. No hadronic events pass the shield and track length selections for upgoing tracks (ignoring their visible scatters). On the basis of this observation, plus the agreement in track range distributions between the UpStop data and the neutrino MC of Fig. 4, backgrounds from non-scattering charged pions and protons are estimated to contribute less than two events to the UpStop data and are hereafter neglected.

5.3 Backgrounds in InDown events

A potential background for InDown events arises from downward, through-going cosmic ray muons whose entrance into the detector was not detected due to a rare episode of poor or non-existent ionization drifting within a calorimeter module. Great care was taken to record all such incidents during data taking and additional checks were made by studying individual module efficiencies as a function of time. A special scan was carried out which rejected events for which there was a possibility of such an occurrence. Additional discrimination against this background was provided by the active shield array, since through-going muons yielded pairs of time-coincident hits having widely separated spatial locations. Using the same minimum track range as was used for the UpStop sample (≥ 260 g/cm^2), no InDown events had $n_{all}^{VS} > n_{trk}^{VS}$. Other backgrounds for PC events were shown to be negligible in Ref. [1], thus the InDown sample was assumed to be background-free in the analysis presented below.

5.4 Event rates

A final sample of 1081 fully reconstructed UpStop-MC events was retained for subsequent analysis. Within this simulation sample, 80% of events originate with neutrino interactions having $E_\nu \leq 10$ GeV. Charged-current quasi-elastic scattering accounts for about one third of the interactions. The neutrino fraction $\nu_\mu / (\nu_\mu + \overline{\nu}_\mu)$ of the sample is 64%.

The numbers of candidate data neutrino events which survive are listed in Table 1, where the MC numbers have been scaled to an exposure of 5.90 fiducial kton-years and include the factor of 0.85 to normalize to the ν_e event rate of Ref. [1]. Comparison of the data with the neutrino MC predictions, the sum of columns 2 and 3, shows that the observed InDown rate is consistent with the prediction, whereas the UpStop data rate appears suppressed by a factor of approximately two. These trends are in agreement with the expectation from the oscillation analysis of Ref. [1]. Note also the small size of the ambiguous sample and the small misidentification rate between the UpStop and InDown samples.

Table 1: Numbers of data and Monte Carlo events which pass all cuts. The no-oscillation MC event rate is normalized to the measured e-flavor event rate of Ref. [1] assuming no oscillations.

Assigned as	*No-osc. MC Truth*		*Data*
	InDown	UpStop	
InDown	12.4±1.4	0.3±0.1	16
UpStop	1.8±0.5	53.3±1.8	26
Ambig	0.8±0.3	3.4±0.4	2

6 Energy and angular distributions of UpStop/InDown neutrinos

The neutrino energy, E_ν, for Monte Carlo UpStop and InDown events is shown in Fig. 7. The UpStop events have an average E_ν of 6.2 GeV. In contrast, the InDown events have lower E_ν values with an average of 2.4 GeV.
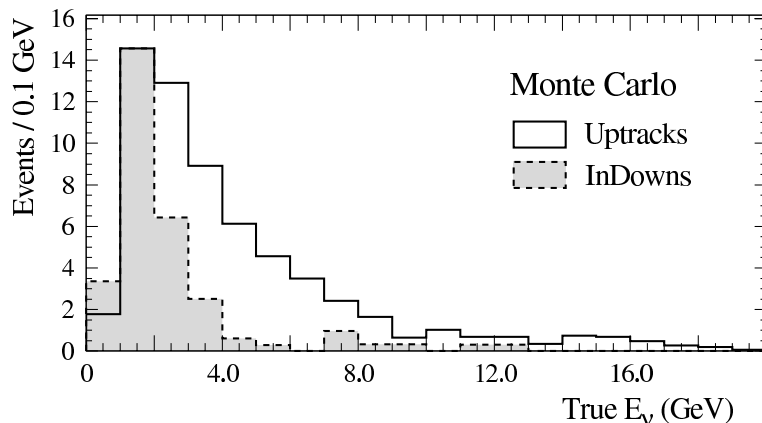

Figure 7: Comparison of the primary E_ν spectra for UpStop and InDown events.

The muon track provides a good estimator for the incident neutrino direction. For UpStop events the average angle between the incoming neutrino and the muon is 11°. For the lower energy InDown sample, the average angle is 13°.

In the likelihood analysis of Ref. [1], the variable $\log_{10}(L/E)$ was used, where L is the neutrino pathlength in kilometers and E is the neutrino final state visible energy in GeV. As demonstrated in Ref. [1], multiple scattering of the exiting muon in PC events allows sufficient neutrino energy determination to permit the reconstruction of the $\log_{10}(L/E)$ distribution. Fig. 8 shows the $\log_{10}(L/E)$ distribution for InDown data (crosses) compared to the no-oscillation MC. The solid-line histogram represents the sum of the partially-contained InDown events from the contained-vertex PC Monte Carlo (PC-MC, dark shading), plus misidentified UpStop-MC events (light shading). Good agreement is observed between the data and the unoscillated Monte Carlo. Hence no evidence is found for oscillations in ν_μ atmospheric neutrinos which are incident from directions above the horizon.
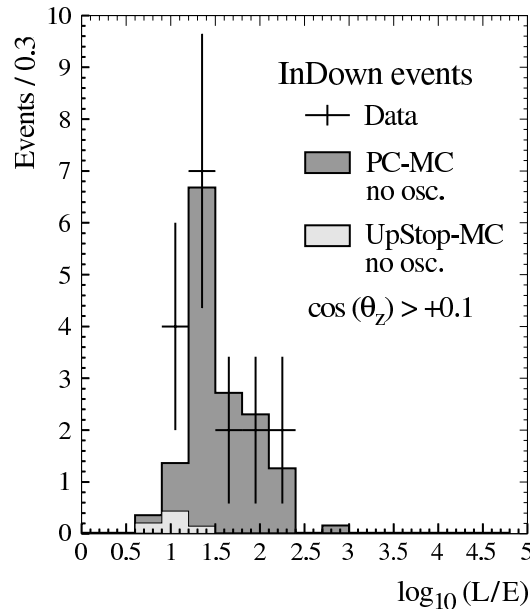

Figure 8: Distribution of $\log_{10}(L/E)$ for the InDown events. The data are shown as crosses; the solid-line histogram shows the neutrino MC expectation for no oscillations. The MC prediction arises mostly from contained vertex PC events (PC-MC, dark shading), but receives a small contribution from UpStop-MC events which were misidentified as InDowns (light shading).

For the UpStop events, however, the whole of the hadronic-shower energy plus a fraction of the muon energy is missing. Thus, whereas L can be calculated accurately from $cos\theta_z$, E is essentially undetermined. The average difference between $\log_{10}(L/E)_\nu$ and $\log_{10}(L/E)_\mu$ is 0.69 (FWHM=0.66), spanning four bins used in the oscillation analysis. Therefore $\log_{10}(L/E)$ is not a useful variable for analysis of oscillations in these events. In this section we show data as a function of $cos\theta_z$. In the analysis described in Section 7 it is convenient to fit as a function of $\log_{10}L$. Fig. 9 shows the distribution of $cos\theta_z$ for upward-stopping muon data events. The distribution decreases steadily towards the nadir. Fig. 9 also includes the simulated UpStop-MC (light shading) and the misidentified contained-vertex PC-MC
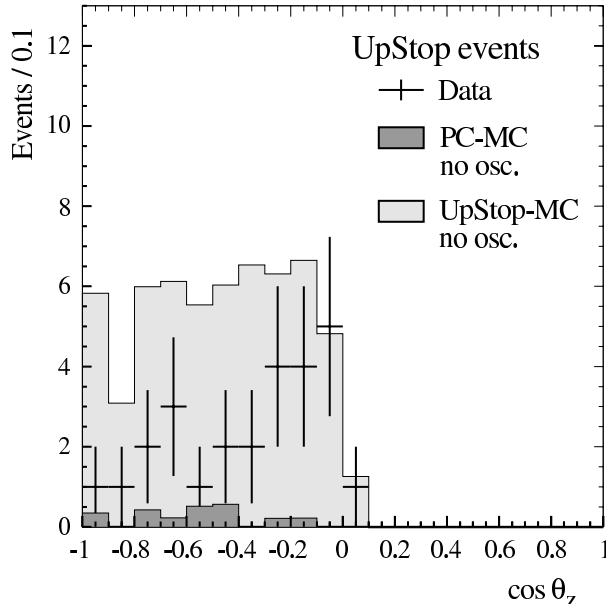
Figure 9: Distribution of cosθ_z for the UpStop events. The crosses represent the data, and the solid-line histogram shows the expected MC distribution for no oscillations. Light and dark-shaded areas show the contributions of UpStop and InDown events for no oscillations.

(dark shading) distributions, for the no-oscillation case. Significant disagreement between the neutrino UpStop events and the no-oscillation expectation is apparent towards the nadir, which is consistent with the loss of upward-going μ-flavor events due to oscillations.

The distributions of Figs. 8 and 9 imply constraints on neutrino oscillation scenarios. These samples have been included in a likelihood analysis together with all the other neutrino events from the experiment. The method and the results of this global fit to Soudan-2 neutrino data are described in Section 7 below.

7   Oscillation analysis

7.1   Outline of the method

The oscillation analysis is a bin-free likelihood analysis based on the prescription of Feldman and Cousins [17]. A detailed description of the method can be found in Ref. [1] and is not repeated here. The main points of the analysis are:

(1) As reported in Ref. [7] and confirmed by Ref. [1], the distributions of neutrino-induced e-flavor data events are consistent with the null oscillation MC predictions, up to an overall normalization. Only the μ-flavor data exhibit oscillation effects. Thus this analysis assumes two flavor $\nu_\mu \to \nu_\tau$ oscillations.

(2) The FC and PC samples described in Ref. [1] are used unchanged in the present analysis. The InDown events are added to the PC muon-flavor sample, and the Ambiguous events

are used only in the overall normalization. The UpStop events are treated as a new category and analyzed as a function of $\log_{10}L$ rather than as a function of $\log_{10}(L/E)$.

(3) A likelihood function for the data is constructed as a function of Δm^2, the mass-squared difference, and of $\sin^2 2\theta$, where θ is the mixing angle, using probability density functions (pdf's) determined from the MC sample. Details of the formalism are given in Ref. [1].

(4) The summed negative log likelihood is evaluated at each point on a 15×80 grid of $\sin^2 2\theta \times \log_{10}(\Delta m^2)$ with $\sin^2 2\theta$ varied between 0.0 and 1.0 and Δm^2 varied between 10^{-5} and 10^0 eV^2. The lowest negative log likelihood on the grid is found and $\Delta\mathcal{L}$, the difference between the lowest value and the value in each ($\sin^2 2\theta, \Delta m^2$) grid square, is plotted.

(5) A background contribution of non-neutrino events arising from neutrons and gammas produced by muon interactions in the rock around the detector is added to the likelihood function. The background contribution only affects the FC events; the PC events and the new InDown and UpStop events are treated as background-free.

(6) The overall normalization of the MC and the amounts of background in the different FC event samples, estimated using shield-tagged data events and the depth distribution of the event vertices, are nuisance parameters whose values are optimized at each grid square.

(7) The allowed confidence level regions are calculated by the method of Feldman and Cousins [17]. That is, MC experiments are generated and analyzed at each grid square to calculate the expected likelihood rise for a given confidence level based on the statistical and systematic errors at that grid square. In addition to the systematic errors described in Ref. [1], a 10% systematic error on the relative normalization of the UpStop events to the remainder of the data was allowed. The latter error represents uncertainties in density and nuclear composition of rock below the detector, and uncertainties with variation of neutrino cross sections in rock versus iron.

(8) The analysis of Ref. [1] used the one-dimensional flux calculation of the Bartol group [12]. This analysis uses their new three-dimensional calculation [13] and compares it with their 1D calculation and with the 3D calculation of Battistoni *et al.* [14].

The 44 new data events documented here are added to the 488 data events of the previous analysis. However, the new events are "high resolution" μ-flavor events, those most sensitive to oscillations, consequently they enhance the sensitivity afforded by the 167 events of that type in the previous analysis.

7.2   Oscillation results

The values of $\Delta\mathcal{L}$ are plotted in Fig. 10 as a function of $\sin^2 2\theta$ and $\log_{10}(\Delta m^2)$. The resulting surface is similar to that reported in Ref. [1]. The main difference is that the likelihood rise for the grid square with the lowest values of Δm^2 and $\sin^2 2\theta$ (called the no oscillation point) is 16.0 compared with 11.3 for the previous analysis. The new data
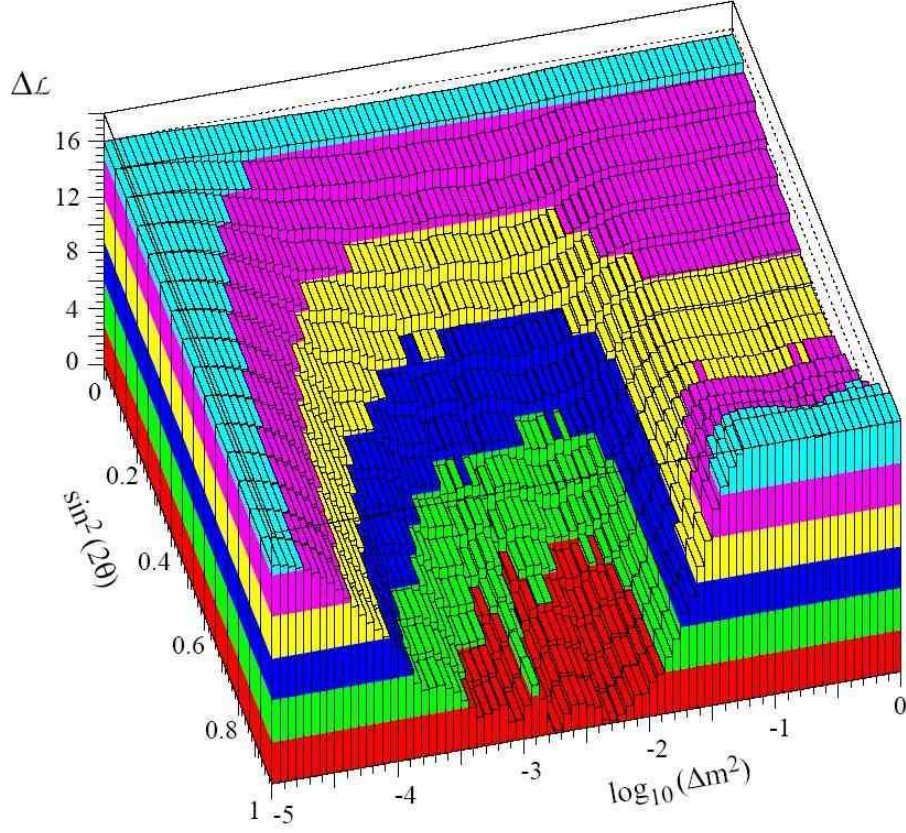
Figure 10: The data likelihood difference, $\Delta\mathcal{L}$, plotted as a function of $\sin^2 2\theta$ and $\log_{10}(\Delta m^2)$.

has significantly increased the discrimination against the no-oscillation hypothesis, mostly because of the large suppression of the UpStop data compared to the MC prediction. The probability of the validity of the no-oscillation hypothesis is discussed in Sect. 7.3.

The $\Delta\mathcal{L}$ surface in Fig. 10 exhibits two nearly equal minima, one at the grid square centered at $\Delta m^2 = 0.0017$ eV^2, $\sin^2 2\theta = 0.97$, and one at $\Delta m^2 = 0.0052$ eV^2, $\sin^2 2\theta = 0.97$. The first minimum is the "best fit point" of this analysis, while the second minimum was the best fit point in the previous analysis [1]. The difference of $\Delta\mathcal{L}$ between the two is only 0.18. There is a small rise in likelihood between the two minima which peaks at about 1.8 in the region of the Super-K best-fit point. However, the 90%-confidence-level limit of this analysis, determined in Sect. 7.3, contains all of the Super-K allowed region. The value of the flux normalization at the best fit point is 91% of the Bartol-3D prediction [13].

Although the analysis is carried out using the log-likelihood function, it is useful to evaluate the goodness of the fit by projecting out the distributions for the various data sets and calculating a χ^2 for the data compared to the MC prediction. Fig. 11a shows the data for the total muon PC sample (including the InDown events) and Fig. 11b shows the UpStop events, compared to the MC predictions.

The PC events are in good agreement with the no-oscillation histogram, but disagree, particularly at low L/E (downward going ν events), with the prediction at the highest
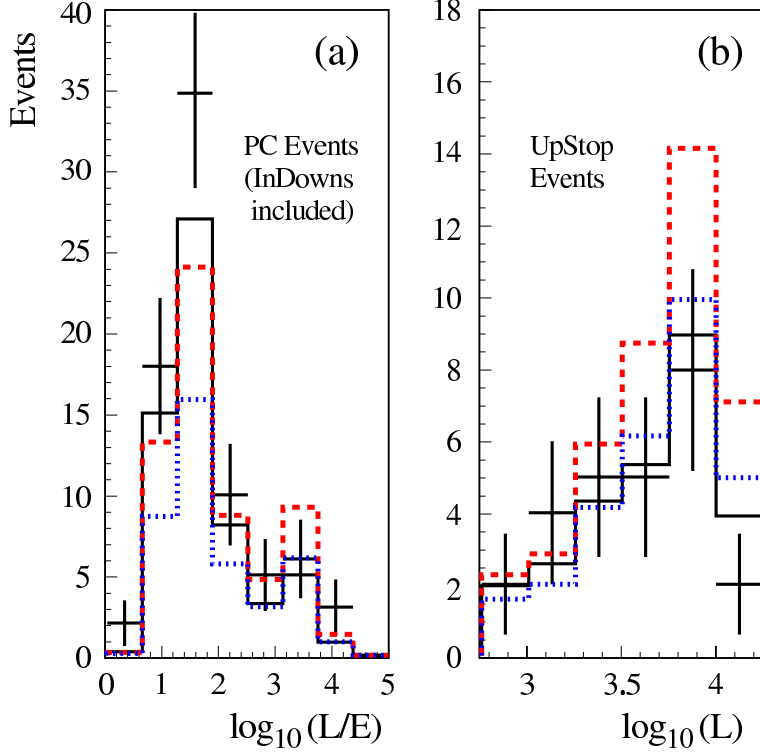
Figure 11: (a) The $\log_{10} L/E$ distribution for the PC event sample that includes the InDown events. (b) The UpStop events plotted as a function of $\log_{10} L$. The points with error bars are the data. The solid histogram is the MC prediction at the best fit point, and the dashed histogram shows the no-oscillation expectation. The dotted histogram depicts "saturated oscillations" with $\sin^2 2\theta = 1.0$, $\Delta m^2 = 1.0$ eV^2.

considered values of Δm^2 and $\sin^2 2\theta$ (~ 1.0 eV^2 and ~ 1.0), where the oscillations have the greatest frequency and largest size (called "saturated oscillations"). On the other hand, the UpStop events are in disagreement with the no-oscillation prediction, particularly at large L, but agree with the saturated oscillation prediction. This behavior is indicative of oscillations with values of Δm^2 in the low 10^{-3} eV^2 region where downward-going neutrinos have not yet oscillated and upward-going neutrinos have saturated oscillations. The best-fit prediction agrees well with both distributions.

Table 2 gives the χ^2 for the comparison of data and MC for the PC and UpStop distributions as well as the full data set including the other distributions described in Ref. [1]. The χ^2 at the best fit point, using all of the data, is 35.6 for 30 data points.

7.3 Confidence levels

The 90%-confidence-level surface $\Delta\mathcal{L}_{90}$ (not shown), generated by the MC experiments under Feldman-Cousins prescription is very similar to that of the previous analysis. Combining the $\Delta\mathcal{L}_{90}$ surface with the data likelihood surface of Fig. 10 gives the solid-line 90%-confidence-level contour shown in Fig. 12a. For comparison, the 90%-confidence-level contour determined previously in Ref. [1] is shown by the dotted line. It can be seen that the allowed

Table 2: The χ^2 for comparisons of the data to various MC predictions for the PC events, the UpStop events, and the full data set.

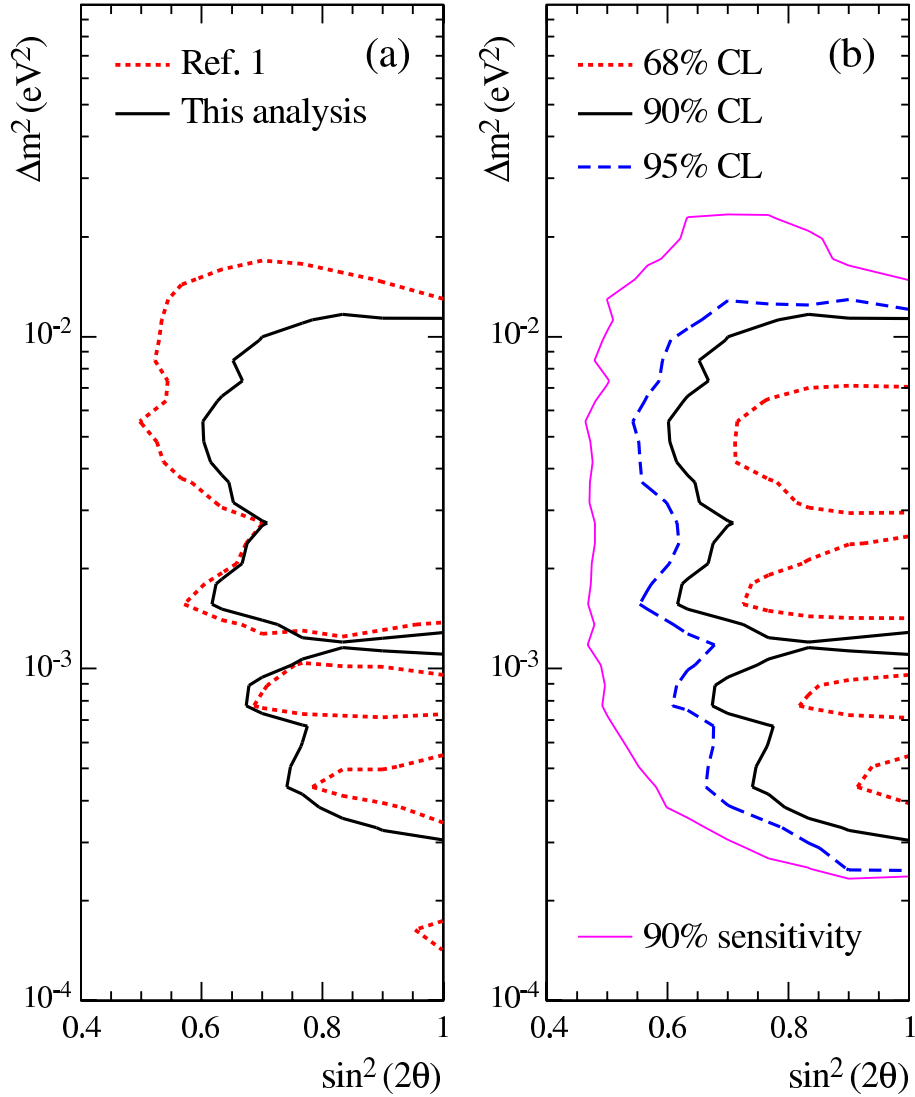|	χ^2/Number of data points		
	PC	UpStop	All data
Best fit	5.0/5	0.6/4	35.6/30
No oscillations	5.9/5	7.9/4	66.6/30
Saturated oscillations	19.8/5	1.9/4	63.2/30

Figure 12: (a) The 90% confidence allowed region from the Feldman-Cousins analysis of this work (solid line), compared to that of Ref. [1] [1] (dotted line). (b) Contours at 68%, 90%, and 95% confidence level (dotted line, thick solid line, and dashed line respectively), compared to the 90% sensitivity contour (thin solid line).

region is more restrictive and that some of the contour structure indicated by the previous analysis has been smoothed. This is due to the fact that the likelihood surface is rather flat at the base of the valley and small changes in the data can move the contours substantially in this region.

Fig.12b shows the 68%, 90% and 95% contours, a further indication of the shape of the likelihood surface. Also displayed in Fig.12b is the 90% sensitivity contour obtained from the Monte Carlo experiments, which denotes the expected 90% contour for experiments with this statistical precision and systematic errors. As was the case in Ref. [1], the 90%-CL contour from this analysis is more restrictive than the estimated sensitivity contour, due, in part, to a small mismatch of the overall event-rate normalization in the electron and muon samples.

The probability of no oscillations can be calculated, under the Feldman-Cousins prescription and including all of the systematic effects, by generating experiments at the minimum Δm^2 and $\sin^2 2\theta$ grid square and counting those MC experiments that give a larger likelihood difference than 16.0. In 500,000 simulated experiments, 16 had a larger likelihood difference giving a probability of 3.2×10^{-5} for the no-oscillation hypothesis.

For UpStop muons and upward-going contained vertex events, the initiating neutrino may experience Mikheev-Smirnov-Wolfenstein (MSW) resonance and other matter effects as a result of the traversal of thousands of kilometers of terrestrial matter. The magnitude of matter-induced deviations from vacuum oscillations was studied using simulated event samples; the samples were weighted in accordance with three-neutrino mixing and the normal mass hierarchy, using the approximation of a uniform (path-weighted mean) terrestrial density [19]. For the range of plausible Δm^2 values, it was found that matter effects, even with maximally allowed mixing angles, can only introduce a few percent additional depletion of muon-flavor neutrinos beyond that which results from $\nu_\mu \to \nu_\tau$ vacuum oscillations [20]. Since the scale of such deviations is well below the statistical sensitivity afforded by the data, matter effects were neglected in this analysis.

7.4   Flux model comparison and event rate normalization

The analysis of this data has been carried out for three different atmospheric neutrino flux calculations: *(i)* the one-dimensional flux calculation of the Bartol group [12], *(ii)* the Bartol three-dimensional calculation [13], and *(iii)* the three-dimensional calculation of Battistoni *et al.* [14]. As well as the flux prediction, the analysis requires an estimate of the height in the atmosphere at which the neutrino is produced. This is particularly important for neutrinos coming from overhead where the path in the atmosphere is a large fraction of the total path length. A parameterization of the pion and muon decay heights was made using the formalism of Ref. [18] for the one-dimensional Bartol calculation. A similar parameterization for decay heights was prepared for the three-dimensional Bartol case. The latter parameterization was also used for predictions based upon the Battistoni *et al.* flux.

Fig. 13 shows the 90%-CL region for the three cases. There is a small change from the one- to three-dimensional flux models, however the three-dimensional models of Bartol and Battistoni *et al.* give almost identical results. The only significant difference between the three cases is in the absolute normalization of the flux. At the best-fit point of this analysis, the normalization factor (number of events observed/calculated) for the Bartol 1D flux is
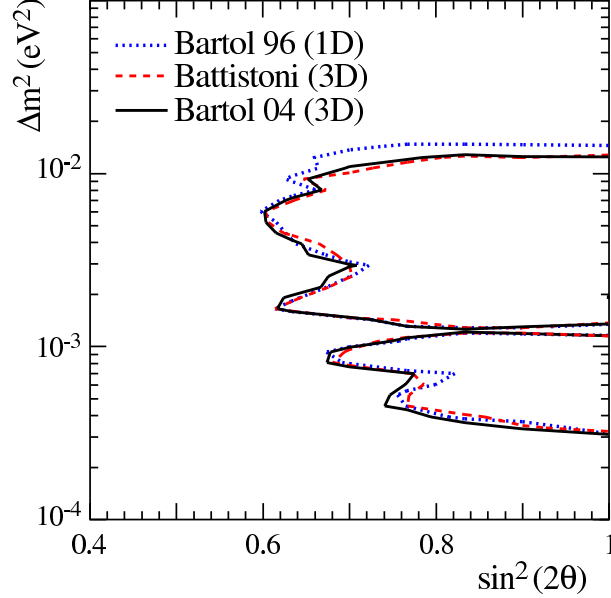
Figure 13: The 90%-confidence-level allowed region for three atmospheric-neutrino flux calculations. The dotted curve is based upon the 1D-model of the Bartol group from 1996 [12]. The more recent 3D calculations of Battistoni *et al.* [14] and of the Bartol group [13] lead to the dashed and solid curve, respectively.

0.86, while for the Bartol 3D flux the factor is 0.91 and for the Battistoni *et al.* flux it is 1.02.

The authors of the flux calculations typically quote large errors of $\pm 20\%$ on the absolute normalization, due to the uncertainties on the incoming cosmic-ray fluxes and on nucleus-air cross sections. There are also significant errors on the neutrino cross sections. It is thus of interest to determine the experimental error on the ratio of the measured to the predicted event rate. The experimental event rate is proportional to the incident neutrino flux, the neutrino cross sections in the detector, and the detector acceptance. This experiment can thus determine the normalization of the atmospheric neutrino flux at the Soudan-2 site times the neutrino cross sections encoded in the NEUGEN3 program [15], for an iron calorimeter with a given energy threshold. Translation of this normalization factor to other experiments at the Soudan site and at other sites is possible in principle. However it requires knowledge of the relative neutrino fluxes at the different sites and the ratio of the neutrino cross sections if a different detector medium or a different neutrino generator is used.

The event-rate normalization factor for Soudan 2 is subject to the following errors:

(1) The total number of neutrino events observed in this experiment above an energy threshold of 300 MeV, obtained from Table I of Ref. [1] and Table 2 of this paper, is 481.2 ± 26.2 ($\pm 5.4\%$). The error includes the statistical error and the error on the background subtraction.

(2) The statistical error on the Monte Carlo sample is $\pm 1.6\%$.

(3) The variation of the fitted normalization factor over the 68% confidence region of the oscillation parameters is $\pm 3\%$. The Feldman-Cousins analysis includes the systematic

errors associated with the background subtraction, cross section uncertainties and energy scale uncertainties.

(4) Depending on the value of θ_{23}, $\nu_e \rightarrow \nu_\mu$ oscillations with the solar parameters could change the flux of ν_e that have traversed the Earth [21, 22]. The change can be positive or negative depending on whether θ_{23} is smaller or greater than 45°. Using the Super-K limits for $\sin^2 2\theta_{23}$ and recent values for the solar oscillation parameters [7, 23], an uncertainty of $\pm 3.3\%$ in the calculated electron-event rate is estimated.

(5) Uncertainty arises in the rate of multi-GeV muon events due to matter effects [20]. A $\pm 1.6\%$ error contribution to the event rate calculation is inferred.

(6) Any mismatch between the Monte Carlo representation of the detector and reality could introduce a relative error in the acceptance of the two and thus an error in the normalization ratio. Detailed studies of individual event channels revealed no significant differences [24, 25]. The relative proportions of different event types and event rejection modes in data versus Monte Carlo samples were studied. A $\pm 2\%$ systematic error, estimated from the maximum differences found between the data and Monte Carlo, has been assigned to account for uncertainties arising from geometric acceptance and other residual effects.

Based upon the $\pm 8\%$ quadrature sum of these errors, an overall normalization factor of 0.91 ± 0.07 is determined for this analysis. This normalization is specific to the Soudan 2 site, the detector medium, the Bartol 3D flux, and to the neutrino cross sections encoded in the NEUGEN3 event generator. It is averaged over the years 1989-2001, one full solar cycle. The same percentage error, $\pm 8\%$, is applicable to the Soudan-2 normalization factors given above for the Bartol 1D and Battistoni *et al.* 3D atmospheric fluxes.

As a check, a normalization which is mostly independent of the $\nu_\mu \rightarrow \nu_\tau$ oscillation parameters can be obtained from the total electron sample of contained and partially contained events. Table I of Ref. [1] lists 208.7 ± 15.9 background-subtracted electron-neutrino events to be compared with an expected rate from the 3D Bartol prediction of 238.1 events, yielding a normalization factor of 0.88 ± 0.07, where the error is just statistical from the number of events and does not include the contribution from $\nu_e \rightarrow \nu_\mu$ oscillations or the other error sources detailed above.

8   Conclusions

Samples of upward stopping muons produced by neutrino interactions in the rock below the Soudan-2 detector and partially-contained events with downward-going muons produced in the detector have been separately isolated. These two new data sets provide additional support and constraints for the hypothesis of atmospheric-neutrino oscillations. The flux of upward stopping neutrino-induced muon events is observed to be suppressed by a factor of approximately two, while downward-going muon events are not suppressed. An oscillation analysis using the method described in Ref. [1] and adding this new data gives a more restrictive 90%-confidence-level allowed region of Δm^2 and $\sin^2 2\theta$. The probability of the no-oscillation hypothesis is reduced by more than a factor of 10, to 3.2×10^{-5}.
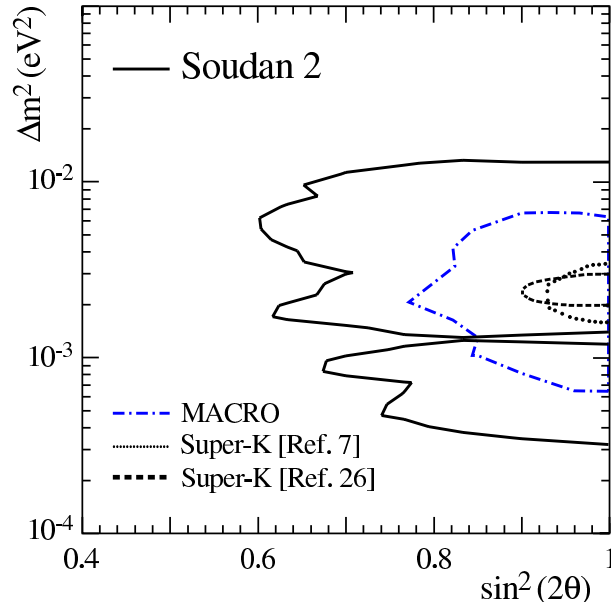
Figure 14: The Soudan 2 90% confidence allowed region in $\sin^2 2\theta, \Delta m^2$ (solid line) compared with the allowed regions of MACRO (dot-and-dashed line) [27], and of the Super-K zenith angle [7] (dotted line) and L/E [26] (dashed line) analyses.

The data have been analyzed using three models of the atmospheric flux at the northern geomagnetic latitude of this experiment. The models include two recent three-dimensional flux calculations and an older one-dimensional calculation. The oscillation parameters are found to be essentially independent of the flux calculation. The normalization factor for the experiment, 0.91±0.07, is the measured event rate divided by the calculated event rate where the latter is the convolution of neutrino fluxes of the Bartol 3D flux calculation with neutrino cross sections encoded in NEUGEN3. The denominator for this ratio contains elements which are specific to the Soudan-2 detector analysis, and site. Consequently, the normalization factor cannot be compared in a straightforward way to other experiments at other geomagnetic latitudes with different detector media and using different neutrino interaction generators.

Comparison of this experiment's revised 90% CL allowed region with the most recent Super-K [7, 26] and MACRO [27] allowed regions is shown in Fig. 14. This result is in good agreement with both experiments.

Acknowledgments

References

[1] Soudan 2 Collaboration, M. Sanchez *et al.*, Phys. Rev. D **68**, 113004 (2003).

[2] MACRO Collaboration, M. Ambrosio *et al.*, Eur. Phys. J. C **36**, 323 (2004).

[3] Kamiokande Collaboration, Y. Oyama *et al.*, Phys. Rev. D **39**, 1481 (1989); S. Hatakeyama *et al.*, Phys. Rev. Lett. **81**, 2016 (1998).

[4] IMB Collaboration, R. Becker-Szendy *et al.*, Phys. Rev. Lett. **69**, 1010 (1992); R. Clark *et al.*, Phys. Rev. Lett. **79**, 345 (1997).

[5] Super-Kamiokande Collaboration, Y. Fukuda *et al.*, Phys. Rev. Lett. **82**, 2644 (1999); Phys. Rev. Lett. **85**, 3999 (2000).

[6] Frejus Collaboration, K. Daum *et al.*, Z. Phys. C **66**, 417 (1995).

[7] Super-Kamiokande Collaboration, Y. Ashie *et al.*, eprint hep-ex/0501064, submitted to Phys. Rev. D.

[8] Soudan 2 Collaboration, W.W.M. Allison *et al.*, Nucl. Instr. Meth. A **376**, 36 (1996); Nucl. Instr. Meth. A **381**, 385 (1996).

[9] Soudan 2 Collaboration, W.P. Oliver *et al.*, Nucl. Instr. Meth. A **276**, 371 (1989).

[10] T. Kafka, H.R. Gallagher, W.A. Mann, J.K. Nelson, Soudan-2 note PDK-803, June 2003.

[11] G. Barr, T.K. Gaisser and T. Stanev, Phys. Rev. D **39**, 3532 (1989).

[12] V. Agrawal, T.K. Gaisser, P. Lipari and T. Stanev, Phys. Rev. D **53**, 1314 (1996).

[13] G.D. Barr, T.K. Gaisser, P. Lipari, S. Robbins, and T. Stanev, Phys. Rev. D **70**, 023006 (2004).

[14] G. Battistoni *et al.*, Astropart. Phys. **12**, 315 (2000); G. Battistoni, A. Ferrari, T. Montaruli, and P.R. Sala, eprint astro-ph/0207035, July 2002. Flux tables for the Soudan site are available at http://www.mi.infn.it/battist/neutrino.html.

[15] G. Barr, D.Phil thesis, University of Oxford, 1987; H.M. Gallagher and M.C. Goodman, MINOS note NuMI-112, Nov. 1995; H. Gallagher, Nucl. Phys. B (Proc. Suppl.) **112**, 188 (2002).

[16] Soudan 2 Collaboration, D. Demuth *et al.*, Astropart. Phys. **20**, 533 (2004); D. M. Demuth, PhD thesis, University of Minnesota, 1999.

[17] G.J. Feldman and R.D. Cousins, Phys. Rev. D **57**, 3873 (1998).

[18] H. Gallagher and K. Ruddick, Soudan-2 note PDK-784, Jan. 2002.

[19] M.C. Gonzalez-Garcia and Y. Nir, Rev. Mod. Phys. **75**, 345 (2003).

[20] W.A. Mann, K. Galdamez, T. Kafka, and A. Sousa, Soudan-2 note PDK-811, Sept. 2004.

[21] O.L.G. Peres and A.Yu. Smirnov, Phys. Lett. B **456**, 204 (1999); Nucl. Phys. B (Proc. Suppl.) **110**, 355 (2002).

[22] W.A. Mann and M. Roberto, Soudan-2 note PDK-807, July 2003.

[23] KamLAND Collaboration, T. Araki *et al.*, Phys. Rev. Lett. **94**, 081801 (2005).

[24] Soudan 2 Collaboration, J. Chung *et al.*, Phys. Rev. D **66**, 032004 (2002).

[25] R.T. Thompson, W.A. Mann, and M.A. Said, Soudan-2 note PDK-791, August 2002.

[26] Super-Kamiokande Collaboration, Y. Ashie *et al.*, Phys. Rev. Lett. **93**, 101801 (2004).

[27] MACRO Collaboration, M. Ambrosio *et al.*, Phys. Lett. B **566**, 35 (2003).